Correlation between Spinning Temperature, Membrane Morphology, and Performance of Psf/PVP/NMP/Water Hollow Fiber Membrane Forming System

Ganpat J. Dahe, Rohit S. Teotia, Jayesh R. Bellare

Department of Chemical Engineering, Indian Institute of Technology Bombay, Powai, Mumbai 400 076, India

ABSTRACT: Asymmetric polysulfone (Psf)/polyvinylpyrrolidone (PVP) hollow fiber membranes were fabricated via dry-wet spinning process in a custom made apparatus with controlled spinneret and spinning lines temperature. This study investigated the effect of isothermal spinning temperatures on morphology, performance, and their relationship. The hollow fibers prepared at isothermal conditions provide greater control over morphology and performance. Thickness of skin at inner side varied with spinning temperature, while morphology at outer cross-section and surface remained same. Three different layers of skin were observed by high-resolution SEM and nodular skin topography by AFM. The viscosity of dope solution was tremendously varied with temperature, which in turn dictates the precipitation rate. Precipitation rate was found to be the controlling parameter for skin thickness. Skin thickness varied from 7.04 to 2.44 μm, as temperature of spinning was changed from 15 to 40°C. The membrane performance was studied by pure water permeability and solute rejection by gel permeation chromatography. Pure water flux increased from 17 to 30 mL/ (m^2 h mmHg) and NMWCO from 13,000 Da to 25,000 Da, with increase in spinning temperature, thereby demonstrating the control of spinning temperature on morphology and membrane performance. © 2011 Wiley Periodicals, Inc. J Appl Polym Sci 124: E134–E146, 2012

Key words: hollow fiber; isothermal spinning; skin thickness; ultrafiltration

INTRODUCTION

The most common technique used for fabrication of ultrafiltration hollow fiber membrane (UF-HFM) is phase inversion method originally invented in 1960 by Loeb and Saurirajan.[1] This method involves numerous spinning parameters *viz.* bore and dope solution compositions, flow rates, etc. making it extremely tedious to reproduce HFMs with a specified morphology and separation performance. Accordingly, it is vital to elucidate the effects of these parameters for optimizing membrane morphology and performance.

The effects of dope solution composition, air gap, bore flow rate, and extrusion pressure on hollow fiber dimension and ultrafiltration performance have been studied earlier. Qin and Chung reported that higher dope flow rate leads to the formation of a hollow fiber with inner porous surface and dense selective layer on outer side which shows reduced water permeability and improved separation. Aptel et al. reported that with decrease in air gap and extrusion rate, the water permeability of polysulfone (Psf) HFM increases while the solute rejection decreases.[2] Further, the addition of polyvinylpyrrolidinone (PVP) and polyethylene glycol (PEG) to polyethersulfone (PES) dope solution increases permeability.[3,4]

Process spinning temperature is an important variable which determines the overall membrane performance. During HFM preparation, a number of steps are carried out either simultaneously or in succession and regulating the temperature at each step is essential. Chou and Yang reported that increasing the coagulation bath temperature from 25 to 70°C increases the water permeability but reduces the solute retention of cellulose acetate hollow fibers, During the process, the outer surface morphology varies from smooth to rough with presence of microvoids.[5] In another study, it was reported that increasing the bore fluid temperature (20–60°C) of polyacrylonitrile HFMs spinning results in enhancement of water flux and reduction in solute rejection without any change in morphology of inner side.[6] Another important aspect is the step at which temperature regulation is carried out. It is known that solvent and nonsolvent diffusion directs the precipitation rate and is directly proportional to absolute temperature. However, nonsolvent diffusion (bore fluid and coagulation bath) does not vary much in these temperature ranges.
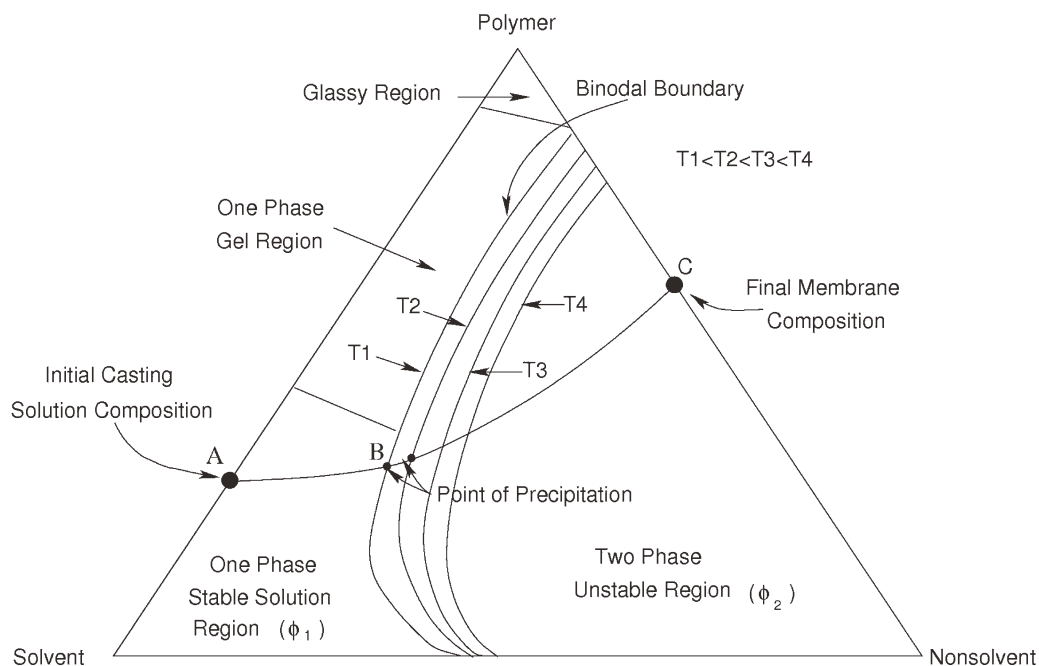
Figure 1 Schematic ternary phase diagram of the binodal curves at various temperatures for ternary system consisting polymer, solvent, and nonsolvent.

Membrane performance depends not only on surface pore size but also on pore length (called as membrane skin). Although the effects of spinning parameters on performance have been extensively studied,[7–12] there are no reports on correlation between spinning temperatures, membrane skin, and separation performance to our knowledge. This may be due to difficulties in identification and differentiation of skin structure from rest of membrane structure.

In this study, we have assessed the effects of spinning temperature on morphology and performance of Psf/PVP composite HFMs. For this, we have designed an experimental set-up to maintain isothermal conditions during spinning keeping all other parameters constant. Observations of membrane morphology have been performed by SEM and FESEM and topography by AFM. Based on these observations, we have quantified membrane skin thickness and correlated it with water permeability and solute rejection. Further, we have also measured the precipitation kinetics of membrane formation based on the macrovoid growth and correlated it with membrane skin thickness.

Phase separation theory using ternary diagram

Membrane skin, which governs HFM performance, is supported on open microporous substrates and its formation is governed by thermodynamic and precipitation kinetics.[13] The thermodynamic influence of spinning temperature can be explained using a ternary phase diagram. Elements of this diagram are the polymer, solvent, and nonsolvent. Commonly used membrane forming additives, such as pore forming agents and surface hydrophilicity/hydrophobicity inducers, when used in dope solution, change the phase system to quaternary. The representation and analysis of a quaternary system is complex, and can be simplified using a pseudoternary phase diagram.

The polymer component of a pseudoternary phase diagram is a mixture of polymer and additive, assuming miscibility between both.[14] Based on Scott's equation, the interaction parameter (χ) between Psf and PVP is 0.29 which indicates homogeneous blending at all concentrations.[15,16] Hence, Psf and PVP mixture can be considered as a single component on a ternary phase diagram. A typical isothermal ternary phase diagram of polymer, solvent, and nonsolvent is shown in Figure 1. Pure polymer, solvent, and nonsolvent are represented by corners of triangle and any point within the triangle represents the respective compositions. The diagram has two distinct regions: one phase (φ_1) and two phases (φ_2). In φ_1, all the components are miscible while in φ_2, solid (polymer-rich) and liquid (polymer-poor) phases are present.

During membrane formation, solvent depletion and nonsolvent intrusion occur in the dope solution which causes composition change from φ_1 to φ_2 by crossing of the binodal boundary. As represented by the line AC, dope solution composition follows the path from point A (initial casting composition) to C (final membrane composition). The composition at point C represents solid matrix (polymer rich phase) of the final membrane, which is in equilibrium with
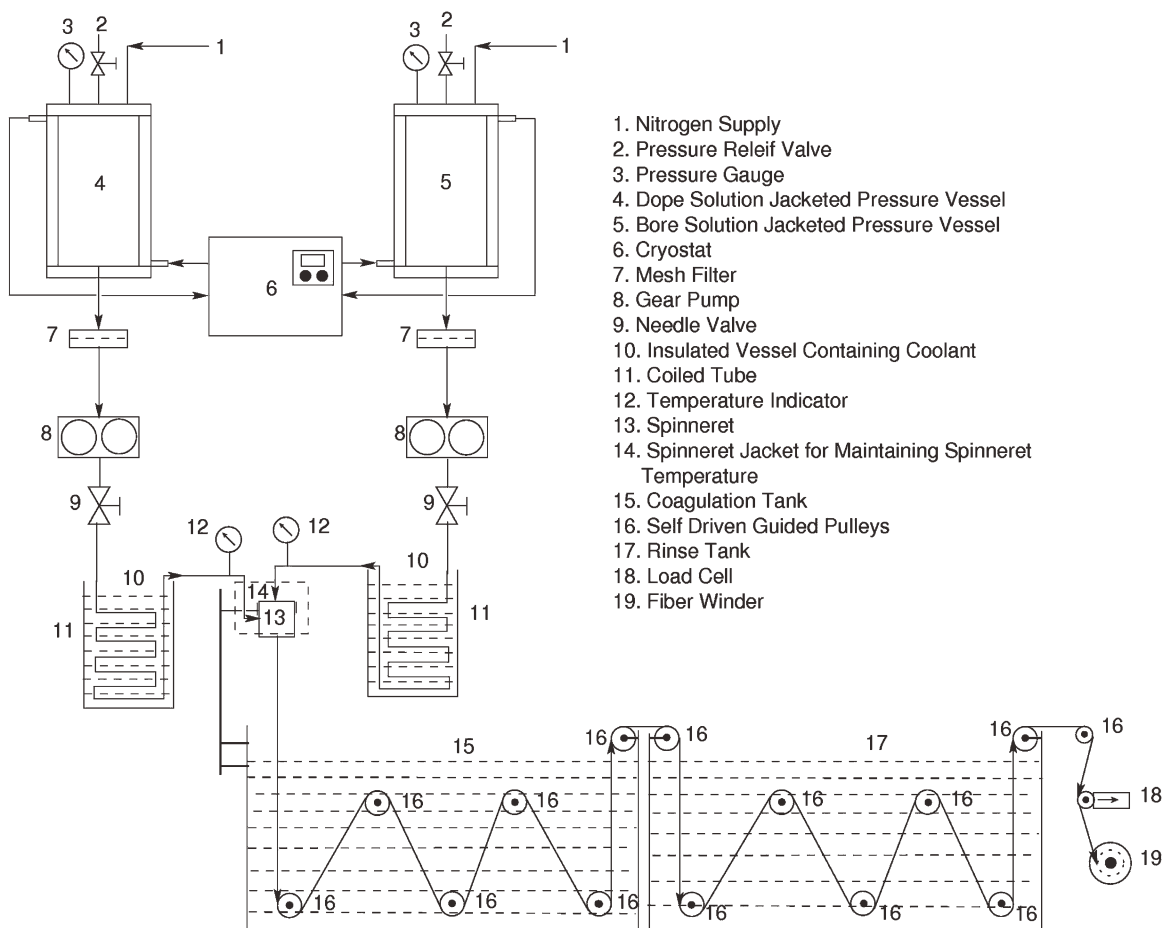
1. Nitrogen Supply
2. Pressure Releif Valve
3. Pressure Gauge
4. Dope Solution Jacketed Pressure Vessel
5. Bore Solution Jacketed Pressure Vessel
6. Cryostat
7. Mesh Filter
8. Gear Pump
9. Needle Valve
10. Insulated Vessel Containing Coolant
11. Coiled Tube
12. Temperature Indicator
13. Spinneret
14. Spinneret Jacket for Maintaining Spinneret
    Temperature
15. Coagulation Tank
16. Self Driven Guided Pulleys
17. Rinse Tank
18. Load Cell
19. Fiber Winder

Figure 2   Schematic of diagram of continuous hollow fiber spinning setup.

the liquid (polymer poor) phase. The position of composition C along polymer-nonsolvent line determines the overall porosity of the membrane.

It is known that the area of φ_2 decreases with temperature.[13] The binodal curves T1, T2, T3, and T4 correspond to different isothermal temperatures such that T1 < T2 < T3 < T4. Since the precipitation paths (AC) and the precipitation rates shall be different for each of these isothermal temperatures, so the spinning temperature is expected to alter the membrane structure, even at the same dope and bore solution compositions. Thermodynamically, the spinning temperature is one of the crucial parameters for defining membrane morphology. It is, however, difficult to trace precipitation path at a particular isothermal temperature on the ternary phase diagram experimentally and correlate it with membrane skin.

EXPERIMENTAL

Materials

Psf (UDEL[TM] P-3500 LCD MB7-BULK) was procured from M/s. Solvay Advanced Polymers, and was dried in vacuum oven for one day at 90°C for re-

moval of absorbed water. PVP (K90) and *N*-methyl-2-pyrrolidone (NMP) were obtained from S.D. Fine-Chem Ltd., India, and used without further purification. The dope solution comprised of Psf/PVP/NMP (20/5/75) and was degassed before the start of spinning to remove dissolved gas. Its viscosity was measured at 15, 20, 30, and 40°C with a CC27/Q1 coaxial cylinder measuring system using an Anton Paar Physica MCR301 Rhemometer (shear rate range, 0.1–10 s^{-1}).

HFM preparation

The hollow fiber was prepared by dry-wet spinning method using a custom-made continuous hollow fiber spinning set-up (Fig. 2). A tube-in-orifice spinneret was used (inner diameter 0.8 mm, outer diameter 1.4 mm). Spinning conditions employed for HFM preparation are indicated in Table I. Special modifications were done to maintain isothermal conditions during spinning. The temperatures of bore and dope lines were monitored continuously by inserting thermocouple junctions directly in the respective lines. Fibers were wound freely without any axial tension. After spinning, the prepared hollow

TABLE I
Process Parameters for Hollow Fiber Membrane Preparation

Ambient temperature (°C)	25
Relative humidity (%)	50–60
Dope solution composition (wt %)	(Psf/PVP/NMP) = 20/5/75
Bore solution composition	Deionized water
Dope solution temperature (°C)	15, 20, 30, 40
Bore solution temperature (°C)	15, 20, 30, 40
Dope flow rate (mL/min)	2
Bore flow rate (mL/min)	2.5
Spinneret ID/OD (mm)	0.8/1.4
Air gap (cm)	38
Coagulation bath composition	Reverse osmosis water
Rinse bath composition	Reverse osmosis water
Coagulation bath temperature (°C)	15, 20, 30, 40
Rinse bath temperature (°C)	25
Take-up drum velocity (m/min)	2.66, 2.66, 3.09, 3.49

fiber membranes were stored in a water bath at room temperature for 1 day to leach the residual NMP.

Morphological study by scanning electron microscopy (SEM)

Morphology studies of HFMs were carried out using scanning electron microscope (SEM). Hollow fibers were fractured in liquid nitrogen and soaked in isopropyl alcohol and hexane. This was followed by coating with gold/palladium using SC7640 Sputter Coater (Quorum Technologies Ltd., UK). The coated samples were observed under electron microscope (Hitachi, S-3400N, UK). High-resolution electron microscopy was performed on a Field Emission SEM (JSM-7600 JEOL, Tokyo, Japan).

Surface topography using atomic force microscopy (AFM)

AFM studies were conducted in tapping mode on the inner surface of hollow fiber using Nanoscope IV equipped with 6626E scanner (Digital Instruments, CA) based on the method described earlier.[17] A silicon nitride probe cantilever was used which had a spring constant of 40 N/m, length 115 to 135 µm, and nominal tip radius of curvature of 8 to 10 nm. The hollow fiber was cut in a small piece along the axis with a small inclined angle and stuck to a metal disk (a puck, 1 cm outer diameter) by double-sided cellophane tape.

Ultrafiltration experiment/pure water permeability

Cross-flow filtration system was used for measurement of pure water permeability (PWP) as shown in Figure 3. The prepared hollow fibers were kept in water bath for 24 h to remove residual solvent in fibers and then immersed in 50 wt % aqueous glycerine solution for 24 h to prevent damage due to the dried structure. Finally, they were dried in air at room temperature for making the test modules.[4] A typical hollow fiber bundle consisted of 16 fibers of 25 cm in length potted in nylon tube of 8 mm diameter with Araldite resin. The glued fiber modules were kept at room temperature for 12 h to cure the Araldite resin completely. After curing, both ends of module along with teflon tube were cut to open the fibers. Residual glycerine was removed by immersing the modules in water for 24 h.

For permeability measurements, the hollow fiber testing modules were fitted in water permeability setup in which deionized water (Milli-Q system, 18 MΩ cm) was pumped at a constant flow rate of 100 mL/min through the lumen of the hollow fibers, using a QD2Q2CKC valve-less metering pump (Fluid Metering, Inc.) and the permeate was collected from shell side. Pressure difference across the membrane module was kept 50 kPa. A coiled Tygon tube was used between discharge point of pump
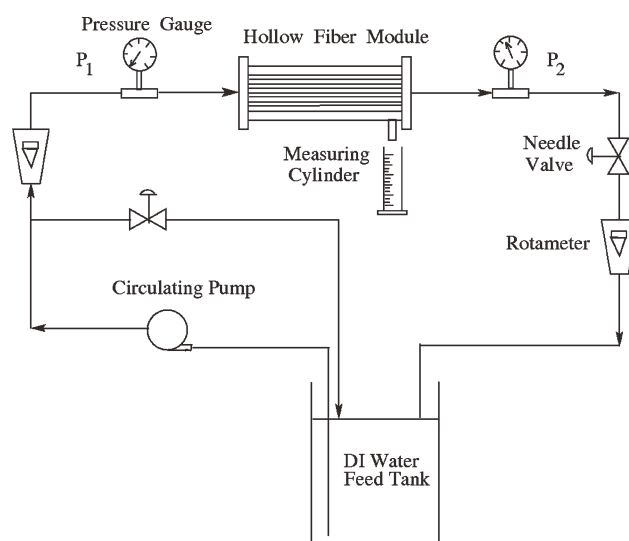

Figure 3 Schematic of setup of pure water permeability (PWP) of hollow fiber module.

TABLE II
Feed Composition of Dextran Fractions

Dextran fraction	MW (kDa)	Suppliers	Concentration (g/L)
T1	1	Pharmacosmos (Holbaek, Denmark)	0.74
T4	4	Serva (Frankfurt, Germany)	1.22
T10	10	Pharmacosmos (Holbaek, Denmark)	0.54
T40	40	Pharmacosmos (Holbaek, Denmark)	0.74
T70	70	Pharmacosmos (Holbaek, Denmark)	0.34
T500	500	Pharmacosmos (Holbaek, Denmark)	0.27
T2000	2000	Pharmacosmos (Holbaek, Denmark)	3.65

and rotameter to nullify flow fluctuations. Pure water permeability (*J*) was calculated using following equation,[13]

$$J = \left(\frac{Q}{n \pi D_i L \Delta P} \right) \quad (1)$$

where *Q* is volumetric flow rate of permeate (mL/min), n is number of hollow fibers, D_i is inner diameter of hollow fiber (cm), *L* is length of hollow fiber (cm), and ΔP is transmembrane pressure (bar). The PWP of each sample was calculated by averaging six readings while the PWP of a set was reported by calculating the average reading of three samples from same run.

Solute rejection/molecular weight cut-off

A feed solution of mixed dextran fractions in deionized (DI) water was used for molecular weight cut-off analysis on the PWP set up by replacing DI water with the feed solution consisting of mixed dextran fractions in deionized water (Table II). Dextran solution was pumped at a constant flow rate of 100 mL/min and pressure 50 kPa across the membrane module at 25°C. The retentate and permeate were recycled through the module for 30 min, sampled, and then analyzed using gel permeation chromatography (GPC) (Waters 1525 binary pumps, Waters 2414 refractive index detector) using two PL aquagel-OH MIXED GPC columns pMIXED-H (8 μm, 300 × 7.5 mm) with a guard column (M/s. Varian BV, Middleburg, Netherlands) in series.[18] The GPC column was calibrated using standard dextran fractions ranging from 1 to 670 kDa (M/s. Pharmacosmos A/S, Holbaek, Denmark) to establish a calibration curve in terms of molecular weight (g/mol) versus retention time (min). Flow rate of mobile phase (DI water) was set at 1 mL/min. GPC chromatograph of dextrans in retentate and permeate was obtained in terms of RI (refractive index) signal verses retention time (min). The rejection curve was then obtained using procedure described earlier.[19,20] Solute rejection was calculated from the following equation,

$$R(MW_i) = \left(1 - \frac{SA_p(MW_i)}{SA_r(MW_i)} \right) \quad (2)$$

where $SA_p(MW_i)$ and $SA_r(MW_i)$ are the slice areas of permeate and retentate at molecular weight MWi, respectively. The selectivity (Φ) of the membrane was calculated from the retention curve by using the following equation,

$$\Phi = \left(\frac{MW(R = 25\%)}{MW(R = 75\%)} \right) \quad (3)$$

For ideal separations, Φ is 1 while for diffuse separations it approaches 0.

RESULTS AND DISCUSSION

Viscosity of dope solution

The dope solution viscosity is significantly influenced by temperature. A plot of dope solution viscosity verses shear rate under temperature variation from 15 to 40°C is shown in Figure 4. The dope solution viscosity significantly increases from 11,000 cP to 33,000 cP as the temperature decreases from 40 to 15°C. This is because of reduction in temperature resulting in reduced chain flexibility and increased
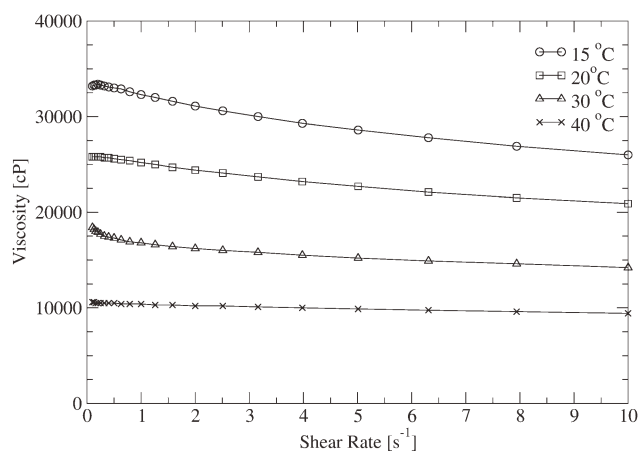
Figure 4 Viscosity plot of Psf/PVP/NMP in a ratio of 20/5/75 dope solution with temperature.
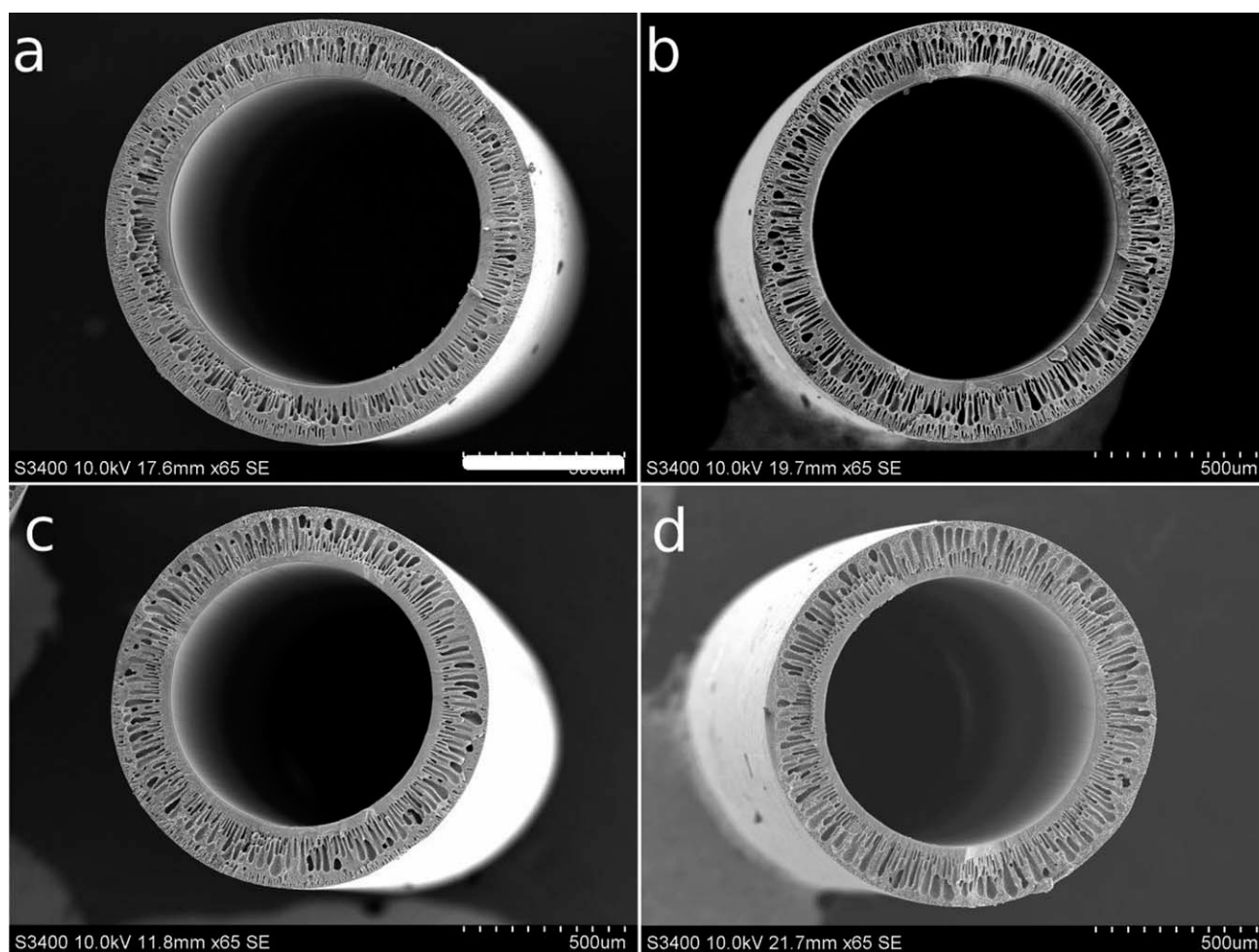
Figure 5 SEM micrograph of cross-section of whole hollow fibers spun at (a) 15, (b) 20, (c) 30, and (d) 40°C. Scale bar 500 μm.

chain rigidity. Further, the shear thinning characteristic of dope solution is more prominent at lower temperatures (15–30°C), while at 40°C it behaves like a Newtonian fluid, as no change in viscosity is found with respect to shear rate.[21]

Morphology of the hollow fiber membranes

The SEM micrographs of whole cross sections of Psf/PVP hollow fibers are shown in Figure 5 and indicate that the HFM inner diameters gradually decrease with increasing spinning temperature, while wall thickness is not considerably affected (Table III). Also, the change in fiber diameter occurs due to gravity-assisted elongation in the air gap and has been reported earlier.[9,22] The only variable parameter across all HFM preparations is the spinning temperature. As discussed earlier, the viscosity of solution rapidly decreases with rise in temperature. So, the elongation increases with decreasing viscosity i.e., it increases with temperature. Thus, the inner diameter of the hollow fiber may get decreased due

to reduction in viscosity. However, no significant change in HFM wall thickness is observed may be because of instantaneous precipitation occurring during the membrane formation.

The cross-sections of one side of the respective HFMs are shown in Figure 6 and indicate varied microstructures from inner to outer side. Macrovoids, large cavities of conical (tear drop) shape having an apex pointing toward the initiating precipitation front, are observed in all cases. The macrovoid formation begins from both inner and outer surfaces for 15 and 20°C spinning temperatures [Fig. 6(a,b)],

TABLE III
Dimensional Change of Hollow Fiber as Function of Temperature

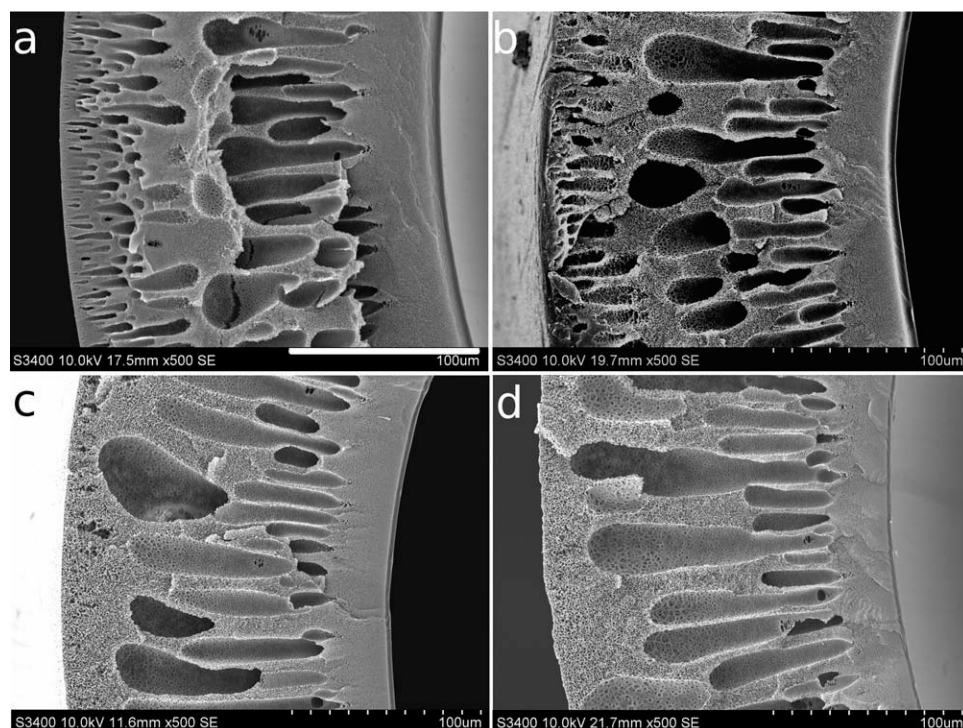| Temperature of spinning (°C)	Inner diameter (μm)	Wall thickness (μm)
15	984	195
20	958	192
30	873	214
40	852	190

Figure 6 SEM micrograph of cross section of one side of hollow fibers spun at (a) 15, (b) 20, (c) 30, and (d) 40°C. Scale bar 100 μm.

while only inner surface macrovoid growth is observed for 30 and 40°C [Fig. 6(c,d)]. This clearly indicates that complete hollow fiber precipitation occurs at 30 and 40°C as it reaches the coagulation bath.

Figure 7 exhibits the formation of a dense structure at inner side which is followed by porous sublayer for all HFMs. The dense structure is typical of selective layer, which can be considered as the membrane skin. Also, the skin thicknesses of HFMs
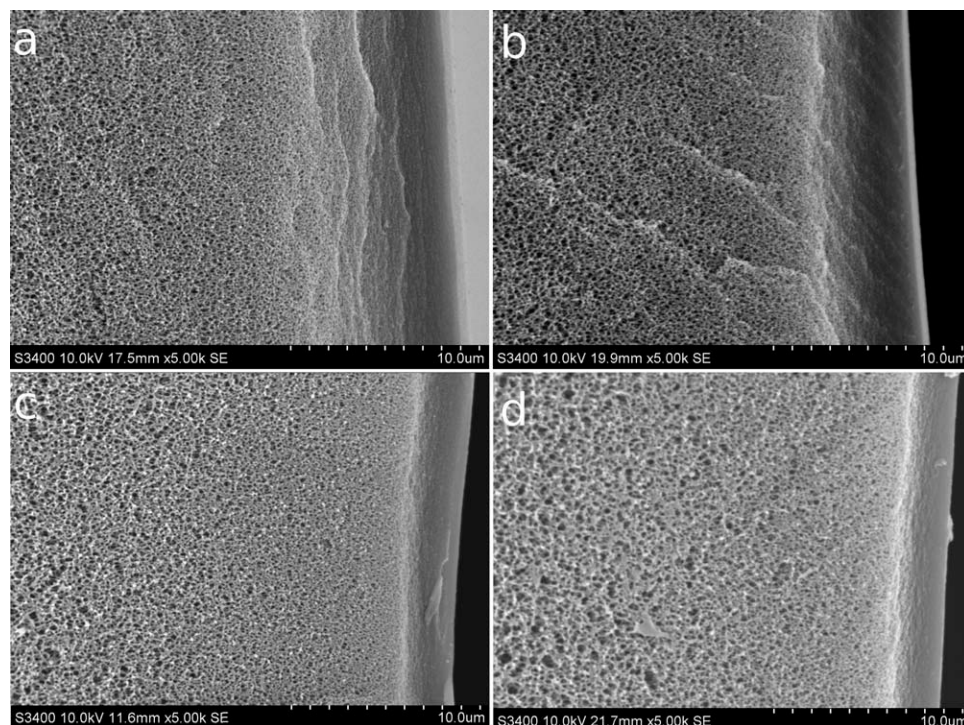
Figure 7 SEM micrograph of cross-section of inner side of hollow fibers spun at (a) 15, (b) 20, (c) 30, and (d) 40°C. Scale bar 10 μm.
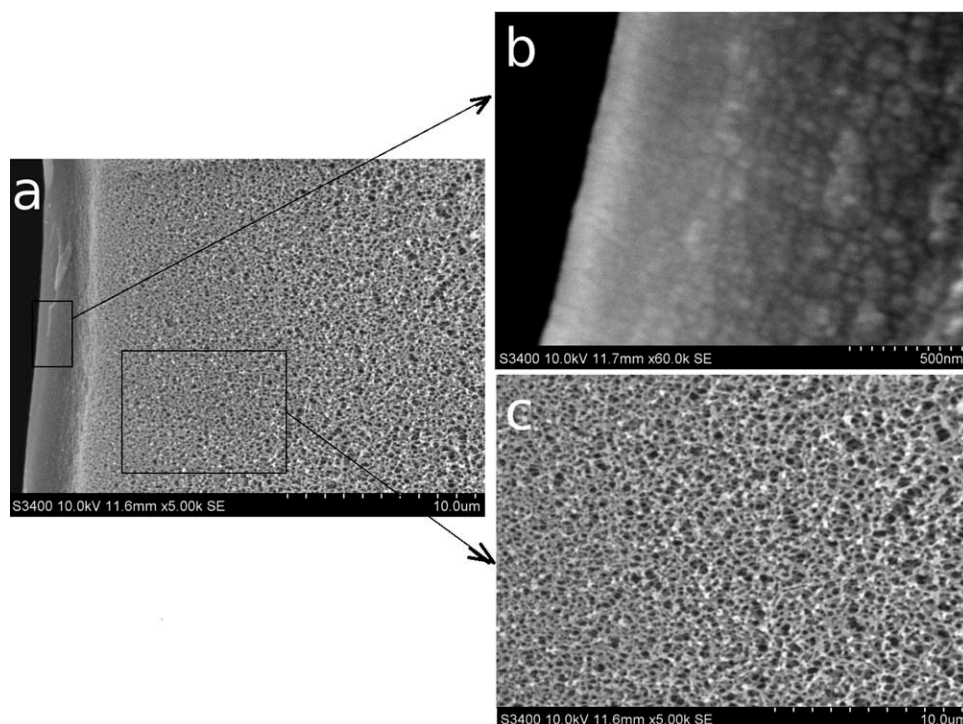
Figure 8 SEM micrographs of inner side of hollow fibers spun at 30°C of (a) ×5000, (b) ×60,000, (c) ×5000.

gradually decrease with increase in spinning temperature. As shown in Figure 8, the skin microstructure of HFM prepared at 30°C consists of a dense structure followed by a lacy structure. The lacy structure is highly porous [Fig. 8(c)] and consists of network formed by beaded polymer strings (connected nodules). The outer sides of all HFMs possess an open cellular structure in the form of highly porous percolating foam as shown in Figure 9. These observations exhibit the
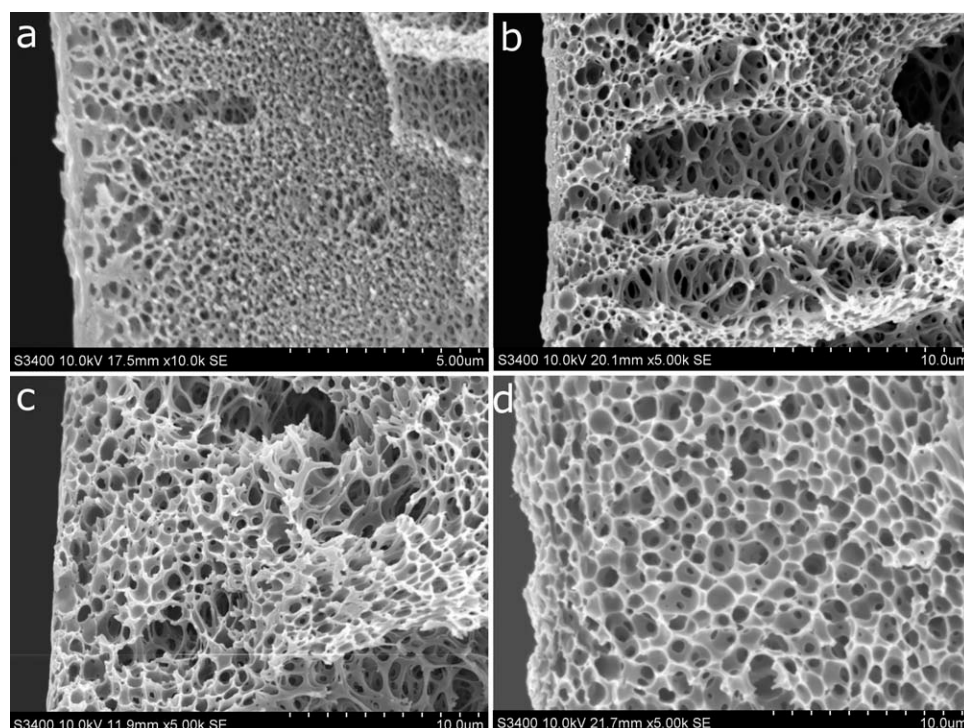

Figure 9 SEM micrograph of cross section of outer side of hollow fibers spun at (a) 15, (b) 20, (c) 30, and (d) 40°C. Scale bar: a, 5 μm and b–d, 10 μm.
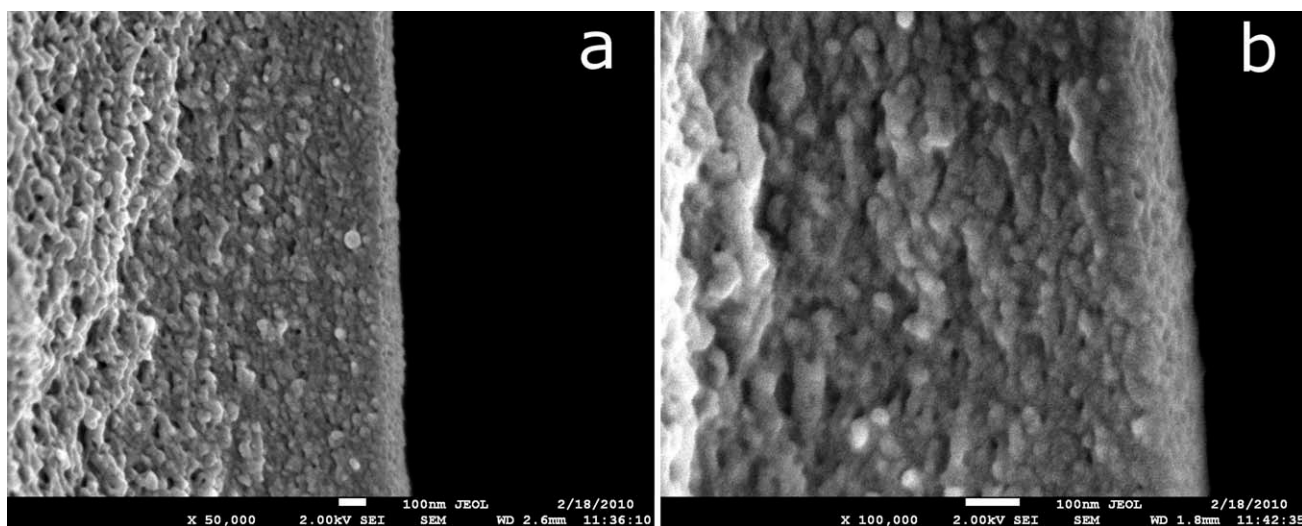
Figure 10 High-resolution electron micrograph of typical membrane skin at (a) ×50,000 and (b) ×100,000.

formation of membrane skin only on the inner side of HFMs.

Analysis of membrane skins

Upon liquid nitrogen based fracturing, a hollow fiber gives different fracture patterns due to its anisotropic structure. Consequently, the denser structure differs in pattern from the loose structure and this phenomenon can be used in identifying the membrane skin. Membrane skin usually consists of a typical nodular morphology as is seen in the high-resolution SEM micrographs (Fig. 10). Also, the nodule sizes increases in direction of the precipitation front.

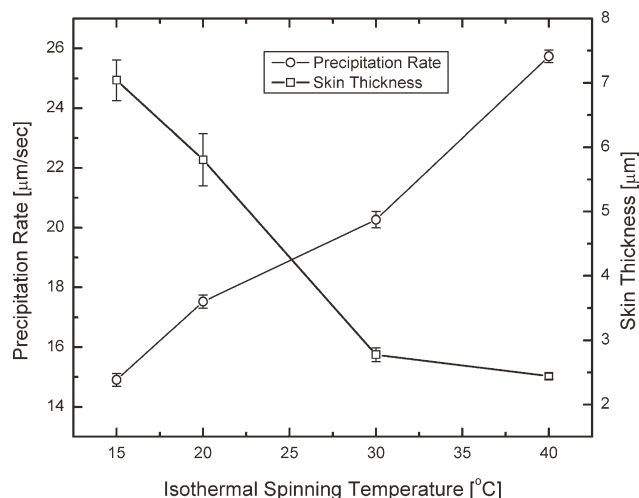The nodule and pore sizes and skin thicknesses of HFMs have been measured by Image J software

Figure 11 Precipitation rate (in air gap) and membrane skin plotted against temperature of the spinning.

(1.41 Version, National Institutes of Health) based on these high resolution SEM micrographs (Fig. 10). The skin consists of three distinct porous layers—the first layer consists of small-sized ($\sim$ 9 nm) pores, the second layer is made up of a tightly-packed nodular structure containing nodules in the size range 25 to 50 nm with no voids and the third layer consists of void-containing networked nodules. Based on cross section measurements (Fig. 7), skin thickness is found to decrease from 7.04 to 2.44 μm upon increasing the temperature from 15 to 40°C. Yong et al. have shown that the precipitation kinetics controls the membrane morphology.[23] Our results exhibit that since the precipitation rate is regulated by viscosity of the dope solution which, in turn, is dependent on the temperature, so by regulating temperature it is possible to control skin thickness.

During HFM preparation, the formation of finger-like or double finger macrovoids is decided by the relative precipitation rates of two precipitation fronts initiated at inner and outer surfaces.[10,24] In case of macrovoid formation at both surfaces, the outer surface precipitation front is initiated when the inner surface precipitation front reaches halfway before entering coagulation bath. The relative precipitation rates can be indirectly measured by observing the macrovoid growth in the membrane.[25] Figure 11 shows precipitation rates of inner front (in air gap) and skin thicknesses plotted against spinning temperature. The precipitation rate is found to increase from 14.91 to 25.75 μm/s as the spinning temperature is increased from 15 to 40°C. This indicates that skin thickness is inversely proportional to precipitation rate.

The precipitation rate depends on solvent and nonsolvent mass transfer, which in turn depends on diffusivity of solvent in nonsolvent and diffusivity
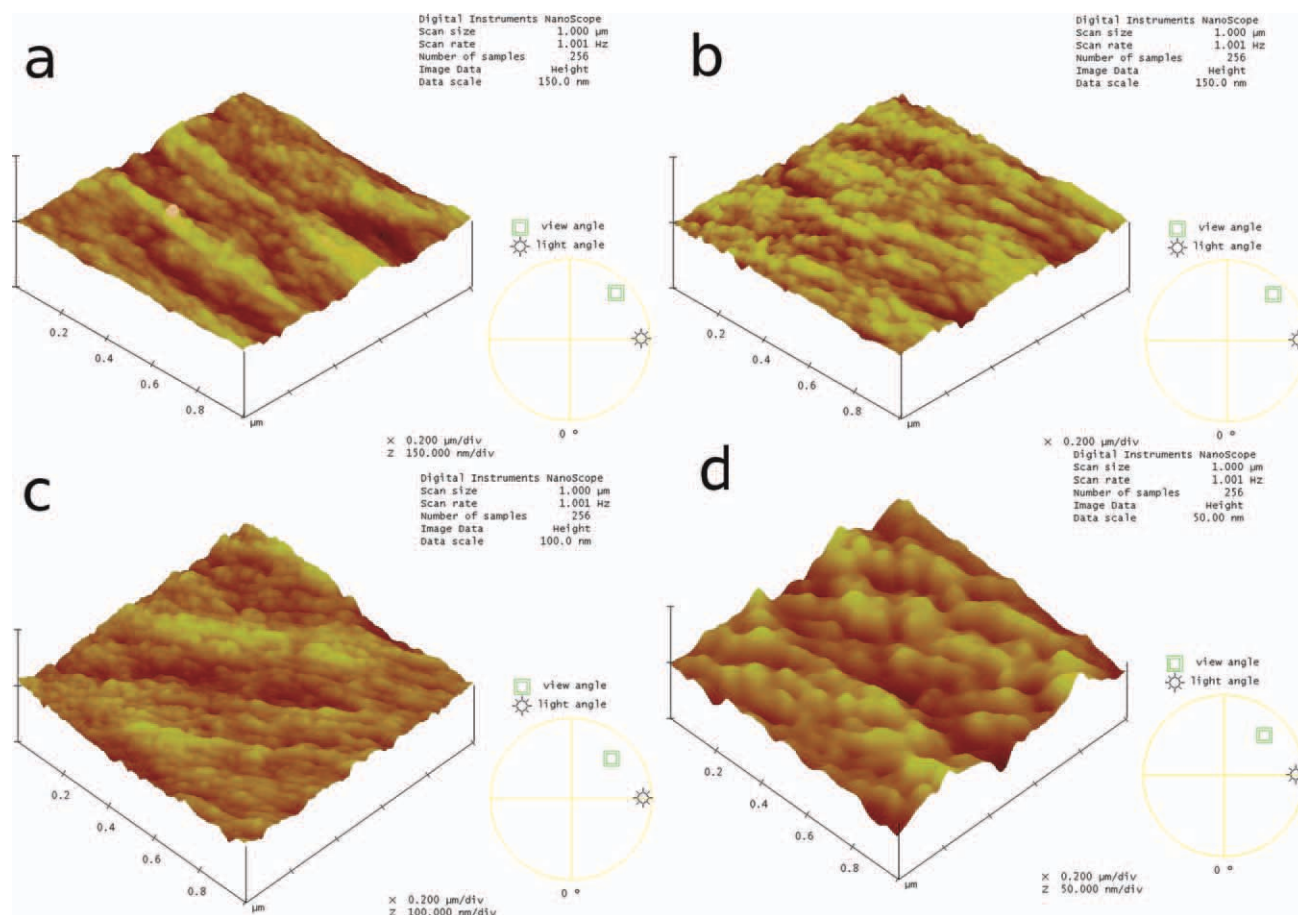
Figure 12 Three-dimensional AFM images of the inner surface of hollow fiber spun at (a) 15, (b) 20, (c) 30, and (d) 40°C. [Color figure can be viewed in the online issue, which is available at wileyonlinelibrary.com.]

of nonsolvent in dope solution (D_{AB}). D_{AB} is a function of temperature and viscosity of polymer solution, and can be related by the Willke-Chang equation.[26]

$$D_{AB} = \left(\frac{(117.3 \times 10^{-18}) \times (\Phi M_B)^{0.5} \times T}{\mu \upsilon_A^{0.6}} \right) \quad (4)$$

where Φ is the association factor for solvent, M_B is solvent molecular weight, T is absolute temperature; μ is solution viscosity, and υ_A is the solute molar

volume at normal boiling point. The correlation indicates that D_{AB} is inversely proportional to the viscosity of dope solution. Temperature has negligible effect on diffusivity of solvent in nonsolvent since the change is small (283–313 K). Hence, D_{AB} is the only factor affecting the precipitation rate.

Surface topography of HFM using AFM

AFM is a promising technique for topographical studies of HFMs due to its high-resolution and quantitative surface measurement. Figure 12 shows the three-dimensional AFM images (1 μm × 1 μm) of inner surfaces of HFMs prepared at 15, 20, 30, and 40°C. The images exhibit that HFM inner surfaces are smooth and consist of packed nodular morphology. The root mean square (RMS) surface roughness have been determined by AFM software and surface nodules and pore sizes by visual inspection of line profiles (Table IV) based on previously reported methods.[25,26] HFM RMS surface roughness decreases slightly while nodule and pore sizes increase with increase in temperature. Ideally, smaller the nodule size, smaller should be the

TABLE IV
Surface Roughness R_q, Surface Nodule Size and Surface Pore Size of the Inner Surface Hollow Fiber Membranes Calculated from AFM Images ($n = 20$)

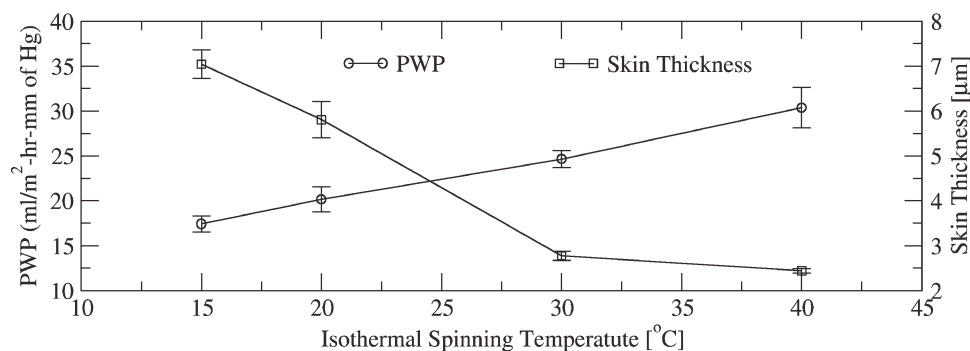| Temperature of the spinning (°C)	Surface roughness (R_q, nm)	Nodule size (nm)	Pore size (nm)
15	6.725	47.23 ± 8.18	36.00 ± 8.75
20	6.826	44.64 ± 7.68	35.58 ± 11.57
30	5.923	46.23 ± 6.03	32.11 ± 6.68
40	4.651	51.10 ± 8.54	42.70 ± 7.07

Figure 13 Pure water permeability and skin thickness of the hollow fibers plotted against temperature of the spinning.
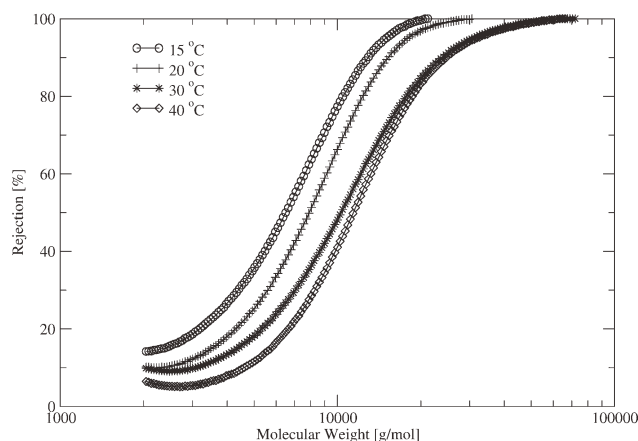

Figure 14 Solute rejection of the fibers spun at 15, 20, 30, and 40°C using dextran feed solution containing fraction 1 kDa to 2000 k kDa.

surface roughness.[17] This, however, is not observed here because AFM measurements are optimized for flat surfaces while some curvature remains for HFMs during flattening. Further, Wienk et al. have proposed that the nodular structure is formed due to spinodal demixing of polymer solution at the non-solvent and dope solution interface, followed by rapid vitrification of the polymer matrix.[27] Hence, solvent and nonsolvent diffusivities are not affected much due to interfacial viscosity. This may be the

reason that there is no significant difference in nodule size and pore size observed at inner surface of the HFM.

Pure water permeability (PWP)

PWP is an important parameter for ultrafiltration HFMs and is strongly dependent on pore size distribution and thickness of the membrane skin. Upon increasing the temperature, PWP increases from 17 to 30 mL/m^2 hr mmHg as shown in Figure 13. However, when the skin thickness is increased, the PWP (J) decreases (Fig. 13). This behavior can be qualitatively explained in terms of the Hagen-Poisseuille equation as,

$$J = \left(\frac{n\pi d^4 \Delta P}{128\mu\delta} \right) \qquad (5)$$

where n is the number of pores of diameter d, δ is the length of the pores (membrane skin thickness), μ is the water viscosity, and ΔP is the pressure difference across the membrane. We have earlier shown that the membrane skin consists of a three layered structure (Figs. 7–9). Out of these, the lacy and open-cellular parts offer negligible resistance to PWP while the packed nodular structure affects it to a large extent. Further, because of no significant
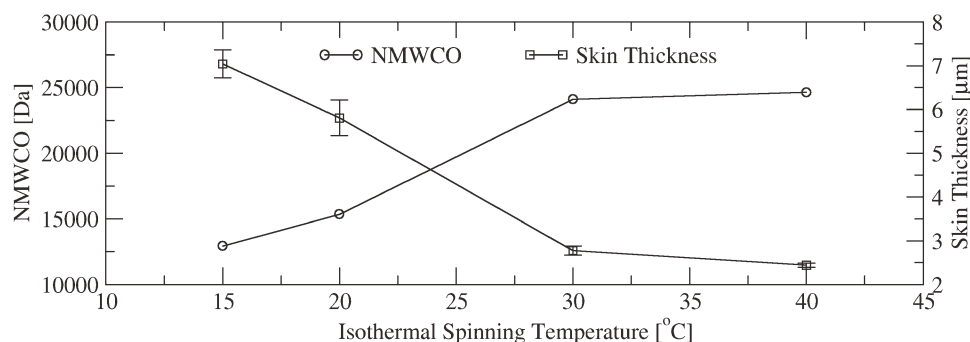

Figure 15 Nominal molecular weight cut off and skin thickness of the hollow fiber plotted against temperature of the spinning.
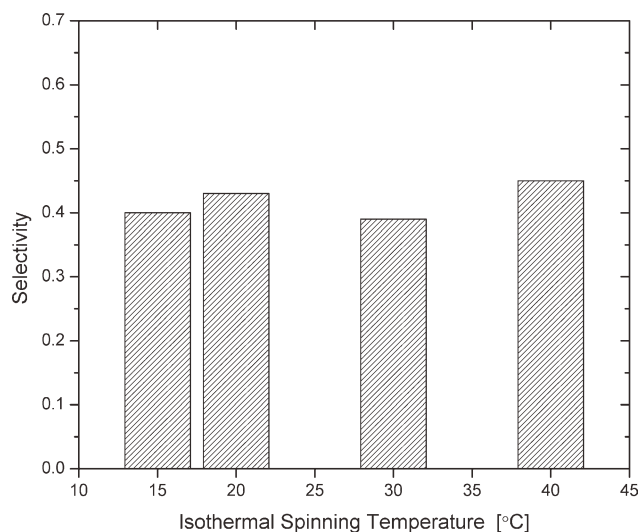
Figure 16 Bar chart of selectivity calculated from solute rejection curve of hollow fiber membrane prepared at 15, 20, 30, and 40°C.

differences in surface nodule sizes as shown by our AFM studies, the surface pore sizes are same for all fibers. Also, since the skin thickness varies with changes in spinning temperature, so PWP is limited only by thickness of the skin.

Solute rejection

The solute rejection profiles of HFMs under temperature increases from 15 to 40°C are shown in Figure 14. Reduction in HFM solute (dextran) rejections is observed as the spinning temperature is increased. The nominal molecular weight cut off (NMWCO) is the molecular weight of the solute which is 90% rejected by membrane under standard conditions. The NMWCO of the HFMs varies from 13,000 to 25,000 Da as the spinning temperature is increased from 15 to 40°C (Fig. 15). Decreasing the spinning temperature enhances the nodule packing length (skin thickness), which in turn improves the separation performance of the hollow fiber.

For ultrafiltration membranes, the pore sizes and pore lengths are not well defined and their combined effects contribute to overall separation performance. In reality, the pore size is the interstitial space between nodules and the pore length is the continuous tortuous space in packed nodule structure. It is known that linear water-soluble polymer molecules like dextran and polyethylene glycol are able to snake-through the membrane pores during separation.[28] An increase in skin thickness means that the solute molecule has to traverse a greater path. Due to this, smaller length polymer molecules can pass more easily than larger ones upon increasing the skin thickness. This may be the reason that molecular weight cut off increases with reductions

in skin thickness. HFM selectivities, as calculated from rejection curves [using eq. (3)], vary from 0.39 to 0.45 as temperature of spinning is changed from 15 to 40°C (Fig. 16). This indicates that selectivity of HFMs is not much affected by skin thickness.

CONCLUSIONS

This study investigated effect of isothermal spinning on morphology and performance of Psf/PVP HFMs. Dope solution viscosity rose sharply when temperature was declined. Precipitation rate decreased with increase in viscosity. Surface pore size in not affected by spinning temperature as from AFM study. SEM study showed hollow fiber with nodular skin, lacy, and open cellular microstructure. Three different skin layers were observed by high-resolution SEM, which in combination dictate the performance. The skin thickness is controlled by precipitation rate and inverse relationship is observed between them. The skin thickness was found to increases with temperature of spinning, while rest of the morphology remains same. Thus, spinning temperature plays crucial role in defining the morphology of HFM. Increased temperature results increase in pure water flux from 17 to 30 mL/m² hr mmHg and NMWCO from 13,000 Da to 25,000 Da. Different NMWCO membranes can be prepared by isothermal spinning without compromising the selectivity. This work can be useful for improving hollow fiber spinning process.

NOMENCLATURE AND UNITS

D_{AB}	Diffusivity of component A into B (m²/s)
D_i	Inner diameter of hollow fiber (cm)
d	Pores diameter (m)
J	Water permeability (mL m⁻² h⁻¹ mmHg⁻¹)
L	Length of the fiber (cm)
M_B	Molecular weight of component B (g/mol)
MW_i	Molecular weight of species i (g/mol)
N	Number of pores (−)
ΔP	Difference across the membrane (bar)
Q	Volumetric flow rate of permeate (mL/min)
R	Rejection (−)
R_q	Surface roughness (nm)
SA_p	Slice area of permeate (−)
SA_r	Slice area of retentate (−)
T	Absolute temperature (°K)

Greek Letters

α	Selectivity (−)
δ	Length of the pores (m)
φ	Phase region (−)
Φ	Association factor (−)
μ	Viscosity (cP)
χ	Interaction parameter (−)

Subscript

i	Species i, inner diameter
p	Permeate
r	Retentate

References

1. Loeb, S.; Sourirajan, S. In Saline Water Conversion-II; American Chemical Society: Washington, D. C., 1963.
2. Aptel, P.; Abidine, N.; Ivaldi, F.; Lafaille, J. P. J Membr Sci 1985, 22, 199.
3. Torrestiana-Sanchez, B.; Ortiz-Basurto, R. I.; Brito-De La Fuente, E. J Membr Sci 1999, 152, 19.
4. Xu, Z. L.; Qusay, F. A. J Membr Sci 2004, 233, 101.
5. Chou, W. L.; Yu, D. G.; Yang, M. C. J Polym Res 2005, 12, 219.
6. Yu, D. G.; Chou, W. L.; Yang, M. C. Sep Purif Technol 2006, 51, 1.
7. Chakrabarty, B.; Ghoshal, A. K.; Purkait, M. K. J Membr Sci 2008, 309, 209.
8. Chung, T. S.; Kafchinski, E. R. J Appl Polym Sci 1997, 65, 1555.
9. Chung, T. S.; Hu, X. J Appl Polym Sci 1997, 66, 1067.
10. Paulsen, F. G.; Shojaie, S. S.; Krantz, W. B. J Membr Sci 1994, 91, 265.
11. Qin, J.; Chung, T. S. J Membr Sci 1999, 157, 35.
12. Chou, W. L.; Yang, M. C. Polym Adv Technol 2005, 16, 524.
13. Mulder, M. Basic Principles of Membrane Technology; Kluwer Academic Publisher: Dordrecht, 1996.
14. Machado, P. S. T.; Habert, A. C.; Borges, C. P. J Membr Sci 1999, 155, 171.
15. Bhattacharya, R.; Phaniraj, T. N.; Shailaja, D. J Membr Sci 2003, 227, 23.
16. Kamide, K. Thermodynamics of Polymer Solutions, Phase Separation and Critical Phenomenon; Elsevier: Amsterdam, 1990.
17. Rafat, M.; De, D.; Khulbe, K. C.; Nguyen, T.; Matsuura, T. J Appl Polym Sci 2006, 101, 4386.
18. Cooper, A. R.; Van Derveer, D. S. Sep Sci Technol 1979, 14, 551.
19. Schock, G.; Miquel, A.; Birkenberger, R. J Membr Sci 1989, 41, 55.
20. Tkacik, G.; Michaels, S. Biotechnology 1991, 9, 941.
21. Bird, R. B.; Stewart, W. E.; Lightfoot, E. N. In Transport Phenomena; John Wiley & Sons, Inc., 2006.
22. Khayet, M. Chem Eng Sci 2003, 58, 3091.
23. Yong, S. K.; Hyo, J. K.; Un, Y. K. J Membr Sci 1987, 60, 219.
24. Frommer, M. A.; Messalem, R. M. Ind Eng Chem Prod Res Dev 1973, 12, 328.
25. Smolders, C. A.; Reuvers, A. J.; Boom, R. M.; Wienk, I. M. J Membr Sci 1992, 73, 259.
26. Treybal, R. E. Mass Transfer Operations, 3 ed.; McGraw-Hill Book Company: New York, 1984.
27. Wienk, I. M.; Van den Boomgaard, T.; Smolders, C. A. J Appl Polym Sci 1994, 53, 1011.
28. Baker, R. W.; Strathmann, H. J Appl Polym Sci 1970, 14, 1197.